MEASURED AND MODELED MORPHOMETRY OF SIMPLE IMPACT CRATERS. W. A. Watters[1] and G. S. Collins[2], [1]Dept. Astronomy, Wellesley College, 106 Central St., Wellesley, MA, USA (wwatters@wellesley.edu), [2]Impact & Astromaterials Research Centre, Dept. Earth Science & Eng., Imperial College London.

Introduction: With the advent of high resolution topography from the Moon and Mars, it is possible to directly compare the shapes of simple impact craters formed in nature and numerical models. Recent improvements to iSALE (Simplified Arbitrary Lagrangian Eulerian for impacts, [1]) include a model of dilatancy which results in a realistic breccia lens forming after the excavation stage [2,3]. Since the shape of simple crater cavities is largely determined by the surface of the breccia lens, these refinements have increased the relevance of model results for understanding simple crater shape and structure [3].

We discuss recent morphometric measurements of well-preserved simple craters on Mars that present a useful test for numerical studies [4]. We also describe preliminary and planned iSALE calculations whose results will be compared with these observations. A primary goal of this work is to examine how the size-dependent scaling of simple crater morphometry depends on physical parameters such as planetary gravity, impactor velocity and mass, and target properties.

Small crater morphometry: Since the pioneering photogrammetric studies of martian crater morphometry in the 1970s-80s [e.g., 5], recent work has largely relied on elevation models derived from laser altimetry and high-resolution stereo imagery [e.g., 6, 7, 8]. We focus here on a recent study that made use of stereo image pairs from the High-Resolution Imaging Science Experiment (HiRISE, [9]) on the Mars Reconnaissance Orbiter (MRO), to characterize the morphometry of well-preserved primary and secondary impact craters on Mars (50 m < D < 5 km) [4,10]. In this study, "good preservation" was identified using a combination of qualitative and quantitative characteristics: e.g., little to no cavity fill, well-preserved and uncratered ejecta, as well as tall rims and deep cavities. Elevation models were generated using the open source Ames Stereo Pipeline [11]. Shape parameters were measured using a custom Python program that first assembles a trace of the rim crest from local elevation maxima, and then extracts non-overlapping radial elevation profiles. Parameter values were computed from individual profiles and subsequently averaged, with uncertainties derived from the azimuthal variation. These quantities include but are not limited to: the ratio of rim-to-floor depth divided by diameter (d/D), curvature radius of the cavity-facing rim wall (λ), cavity shape exponent (α, exponent of power-law fit to cavity cross-section), and upper cavity wall slope nearest the rim (φ).

Terrain and diameter dependence: We expect the following conclusions from this work to be expressed in numerical models of simple crater formation: (a) craters forming in high-strength targets have deeper cavities and taller rims, on average, as found in previous studies of larger craters [e.g., 6, 7]. (b) The slope of the upper rim wall (20% of crater radius nearest the rim and facing the cavity) steepens to critical repose angles for craters exceeding a diameter of ~1 km (see Fig. 1). (c) Also at this diameter, a significant fraction of craters exhibit a general flattening of the upper rim wall (curvature radius λ departs a power law trend), indicating a size-dependent transition in rim shape that may represent additional rim wall collapse. (d) Crater cavities exhibit a relatively conical shape at small diameters (α nearer 1 for D < 200 m) and become more parabolic in cross-section ($\alpha \approx 2$), on average, as D approaches the simple-complex transition diameter (where failure of upper cavity walls lead to flatter floors and $\alpha > 2$; see Fig. 2) .

A prior study found the diameter dependence for cavity wall slopes of fresh-appearing lunar craters using Apollo images: maximum slopes increase with D until the simple-complex transition diameter [12].

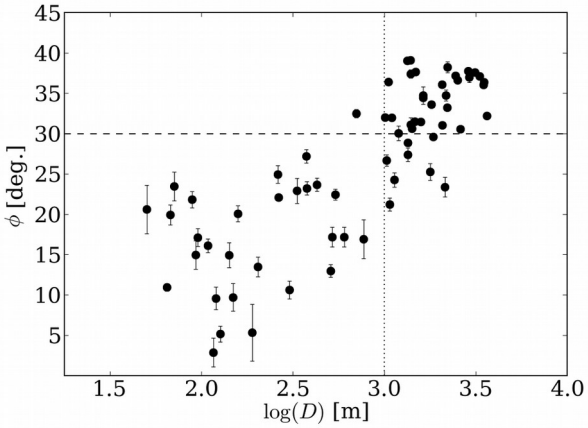

Fig. 1: Upper wall slope vs. log crater diameter D for N=70 well-preserved simple craters on Mars. Typical repose angles (above dashed line) occur for D > 1 km (dotted line). [4]

Odessa- vs. Barringer-style crater growth: We can summarize many of the size-dependent trends by noting that crater walls steepen – especially near the rim – as the cavity becomes more bowl-shaped with increasing crater diameter. This may be a result of the

transition in cratering regimes from the conical "Odessa style" of crater formation that is dominated by radially-directed displacement, versus the excavation-dominated "Barringer-style" crater growth that results from deeper coupling at higher impact energies [13, 14]. In addition to the morphometric trends described above, previous field studies of crater structure have noted circumferential anticlines in Odessa-style craters and overturned flaps in Barringer-style craters [13-15]. As a fraction of cavity volume, Odessa Crater has a much smaller breccia lens.

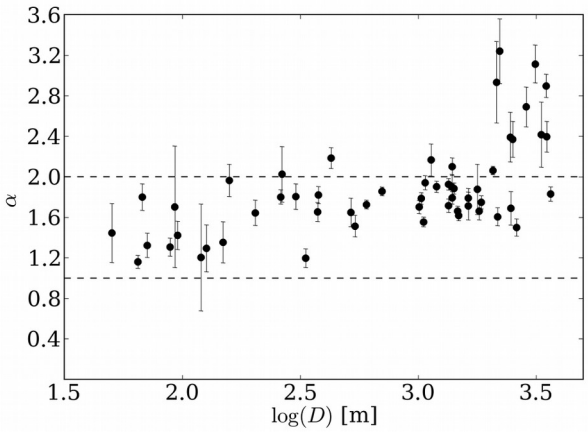

Fig. 2: Exponent of power-law fit to cavity cross-section for *N*=55 well-preserved simple craters on Mars. Upper and lower dashed lines correspond to paraboloidal and conical cavity shapes, respectively. (Adapted from a figure in [4].)

iSALE simulations: We have computed a small preliminary set of simulations using the iSALE shock-physics code without dilatancy to characterize morphometric trends. For a vertically-directed basalt impactor that is 10 m in diameter under conditions of martian gravity impacting a basalt target (with an intact rock strength model [16]), we have examined results for impact velocity ranging from 0.5 to 15 km/s. Example radial elevation profiles of craters formed in the low- and high-velocity regimes are shown in Fig. 3, normalized by crater radius *R*. The observed trend is broadly consistent with the progression outlined above, with slopes steepening near the rim as energy increases and a tendency toward a bowl shape. By contrast, the low-velocity impacts produce shallow, flat-floored craters. For impact velocity v_i = 1 km/s, we find $d/D \approx 0.15$, barely in excess of the ratio measured for Zunil secondaries ($d/D \approx 0.13$) thought to impact at roughly 1 km/s for a downrange distance of 300 km into young lava plains [10]. It should be emphasized that these results are preliminary as many more calculations are required to evaluate the effects of grid configuration and size, boundary conditions, and axisymmetry.

Planned calculations. Our goal is to compute the trends in morphometric parameters from model craters as a function of final crater size under lunar and martian conditions, alternately varying impactor velocity and impactor diameter. These calculations will be carried out with and without dilatancy, for basalt as well as a weaker regolith target. As mentioned, these results will be used to make a detailed comparison with the measurements described earlier and others being acquired. If trends and transitions previously observed on Mars are accurately reproduced in the model calculations, the results for lunar conditions may supply a useful prediction that can be tested with future measurements. Alternatively, the results may offer useful insights into model limitations and can lead to further refinements.

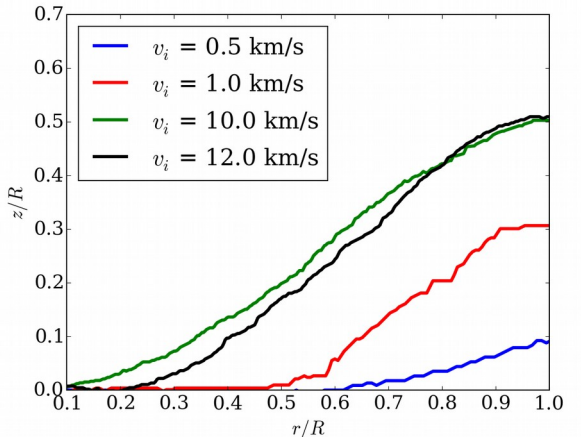

Fig. 3: Radial elevation profiles for iSALE impact simulations carried out under martian gravity, for projectile diameter 10 m over a range of impact velocities in an intact basalt target. Distances normalized by crater radius *R*.

References: [1] Wünnemann K. et al. (2006) Icarus, 180, 514-527; [2] Collins G. S. (2014) *JGR*, doi: 10.1002/2014JE004708. [3] Collins G. S. (2015) *LPSC 46*, #1342; [4] Watters W. A. et al., (2015) *JGR*, doi: 10.1002/2014JE004630; [5] Pike R. J. (1980) LPSC, *11*, 2159-2189. [6] Stewart S. & Valiant G. (2006) *Meteor. Planet Sci.*, *41*, 1509-1537; [7] Whitehead J. et al. (2010) *GSA special papers*, *465*, 67-81; [8] Robbins S. & Hynek B. (2013) *Planet. & Space Sci.*, *86*, 57-65; [9] McEwen A. et al., (2007) *JGR*, *112*, E05S02; [10] Watters W. A. & Radford A. (2014), *LPSC 45*, #2836; [11] Moratto Z., et al., (2010) *LPSC 41*, #2364; [12] Pike R. J. (1977) *Impact & Explosion Cratering*, 489-509; [13] Shoemaker E. M. (1960) *Int'l Geo. Cong. 21*; [14] Shoemaker E.M. & Eggleton R.E., (1961) *Lawrence Radiation Crater. Symp.*, *1*, A1–A27; [15] Shoemaker E. M. et al. (2005) *Aus. J. Earth Sci.*, *52*, 529-544; [16] Collins G. S. et al. (2004) *Meteorit. & Planet Sci.*, 39 (2), 217-31.